PCCP

PAPER

Emission spectroscopy of a ruthenium(II) polypyridyl complex adsorbed on calcium niobate lamellar solids and nanosheets†

Kazuhiko Maeda,* Takayoshi Oshima and Osamu Ishitani

Ru(II) tris-diimine complexes are known to exhibit emission at around 630 nm as a result of ^{1}MLCT photoexcitation. The emission is quenched in the presence of a suitable semiconductor solid due to electron injection from the excited state of a Ru(II) complex to the conduction band of the adjacent semiconductor. Here we investigated emission quenching behaviour of $Ru^{II}\{(4,4'-(CH_3)_2-bpy)_2(4,4'-(CH_2PO_3H_2)_2-bpy)\}$ (bpy = 2,2'-bipryridine) adsorbed on $HCa_2Nb_3O_{10}$ solids having an ordered lamellar structure or a disordered nanostructure. Even though electron injection from the excited state of the Ru complex to the conduction band of nanostructured $HCa_2Nb_3O_{10}$ is thermodynamically less favorable than that of layered $HCa_2Nb_3O_{10}$, faster electron injection was observed using nanostructured $HCa_2Nb_3O_{10}$. Experimental results highlighted that electron injection from the excited Ru complex takes place not only in the conduction band of $HCa_2Nb_3O_{10}$ but also mid-gap states whose density is strongly dependent on both the morphological feature and the preparation method of $HCa_2Nb_3O_{10}$.

Introduction

Electron injection from the excited state of dyes or metal complexes into a semiconductor metal oxide is fundamentally important as the primary process of dye-sensitized solar cells and photocatalytic hydrogen evolution.[1–13] Electron injection efficiency is known to depend on the conduction band potential (E_{CB}) of a metal oxide. For example, efficient electron injection from the excited state of N3 dye into TiO_2 was observed, while that into ZrO_2 having much more negative E_{CB} was very slow.[4] Maitani *et al.* recently observed different charge injection behaviours of the excited state of anthracene dyes on TiO_2 nanocrystals, which originated from different facets of TiO_2 with different energies.[14]

We have studied metal oxide nanosheets as building blocks for dye-sensitized H_2 evolution in combination with ruthenium(II) polypyridyl complexes as redox photosensitizers.[10–13] Ruthenium(II) tris-diimine complexes exhibit emission at around 630 nm as a result of ^{1}MLCT photoexcitation, and the efficiency of electron injection can be assessed by monitoring emission behaviour of the adsorbed Ru complex.[11–13] According to our recent study on time-resolved emission spectroscopy, it was suggested that electron

injection from the excited state of $Ru^{II}\{(4,4'-(CH_3)_2-bpy)_2(4,4'-(CH_2PO_3H_2)_2-bpy)\}$, abbreviated as **Ru** for simplicity, occurs not only in the conduction band of $HCa_2Nb_3O_{10}$ nanosheets but also mid-gap states.[14] If this is the case, the charge injection process should depend on the structural feature of $HCa_2Nb_3O_{10}$. It is fundamentally interesting to investigate emission behaviour of a ruthenium(II) polypyridyl complex on a semiconductor solid having different morphological features. While there have been several reports on emission spectroscopy of metal-complex/semiconductor hybrids focusing on different metal complexes and semiconductors,[14–17] such structural effects of a metal oxide on the emission behaviour have not been investigated so far.

In this work, we investigated structural effects of $HCa_2Nb_3O_{10}$ on the electron injection from the excited state of **Ru** by means of steady-state emission spectroscopy and time-resolved emission spectroscopy. Two types of $HCa_2Nb_3O_{10}$ having distinct morphological features were synthesized: one is a submicron-order layered crystal and the other one is aggregated nanosheets with highly disordered structures, which was prepared by chemical exfoliation of the corresponding lamellar solid. In addition, we applied two different synthetic methods to prepare $HCa_2Nb_3O_{10}$ having different physicochemical characteristics. The details of the materials preparation are included in the experimental section. Briefly, layered $HCa_2Nb_3O_{10}$ was obtained by ion-exchange reaction of $KCa_2Nb_3O_{10}$, which was prepared by a conventional solid-state reaction (SSR) or the polymerized complex (PC) method, with HNO_3. Tetra(*n*-butyl)ammonium hydroxide (TBAOH), a bulky base molecule, was used to exfoliate layered $HCa_2Nb_3O_{10}$ into

Department of Chemistry, Graduate School of Science and Engineering, Tokyo Institute of Technology, 2-12-1-NE-2 Ookayama, Meguro-ku, Tokyo 152-8550, Japan. E-mail: maedak@chem.titech.ac.jp

† Electronic supplementary information (ESI) available: Additional spectroscopic and characterization data. See DOI: 10.1039/c5cp02050f

unilamellar colloidal nanosheets. The TBA$^+$-stabilized Ca$_2$Nb$_3$O$_{10}^-$ nanosheets were flocculated by adding HCl, followed by washing with H$_2$O and drying at 343 K overnight.

Results and discussion

Fig. 1A shows typical SEM images of layered HCa$_2$Nb$_3$O$_{10}$ and the aggregated nanosheets prepared by the PC method. After exfoliation of lamellar HCa$_2$Nb$_3$O$_{10}$ and subsequent restacking by HCl, the original plate-like layered structure was completely destroyed, giving aggregated solids with a disordered structure. This result is also supported by XRD (Fig. 1B), which indicated that long-range ordering in the stacking direction (reflections from (00n)) of the original layered material disappeared after the exfoliation-restacking process. Accompanied by this structural change, the specific surface area determined by nitrogen adsorption at 77 K was increased from 2.4 to 49 m^2 g^{-1}.

Fig. 1C shows UV-visible diffuse reflectance spectra of the same samples, along with an absorption spectrum of a **Ru** solution. Layered HCa$_2$Nb$_3$O$_{10}$ shows a steep absorption edge at around 350 nm, which is due to electron transition from the valence band formed by oxygen 2p orbitals to the conduction band that consists of empty orbitals of niobium 4d. On the other hand, there are at least two absorption edges in the aggregated HCa$_2$Nb$_3$O$_{10}$ nanosheets, both of which are blue-shifted compared to that in the parent layered solid. This is most likely due to a quantum-confinement effect.[18] As discussed in our previous paper, the generation of two absorption edges after the exfoliation–restacking process would result from an increase in the distortion of the two-dimensional nanosheet structure that consists of triple perovskite slabs having a

nanosized thickness. This more pronounced distortion might alter the local structure of NbO$_6$ octahedra in the perovskite block, although the long-range ordering in the perovskite block (shown in XRD) appears to be maintained. Although the precise determination of the band-edge positions of the aggregated HCa$_2$Nb$_3$O$_{10}$ nanosheets appears to be difficult, one may think that the valence band maximum and the conduction band minimum of HCa$_2$Nb$_3$O$_{10}$ are shifted downward and upward, respectively, thereby leading to band-gap widening, as the result of nanostructuring.[19]

Using the two structurally different materials but with almost the same composition, the adsorption of **Ru** was performed by dispersing the solid materials in an aqueous solution containing **Ru** (2.0 μmol g^{-1}). UV-visible spectroscopy showed that the dissolved **Ru** complex was quantitatively adsorbed on the surface of both materials. Note that, however, intercalation of **Ru** into the gallery space of these solids does not occur, as revealed by our previous work.[11,13] As shown in Fig. S1 (ESI†), modification of HCa$_2$Nb$_3$O$_{10}$ material with **Ru** resulted in the generation of a new absorption band centred at around 460 nm, which is due to MLCT transition of **Ru**, identical to **Ru** in MeCN solution (Fig. 1C).

As reported previously,[13] **Ru** on Al$_2$O$_3$ gives an emission peak at around 630 nm as a result of ^{1}MLCT photoexcitation of **Ru** at 444 nm, with a quantum yield of *ca.* 5.6% (Fig. 2). However, the emission was almost completely quenched when **Ru** was loaded on HCa$_2$Nb$_3$O$_{10}$ regardless of the structural feature. This indicates the occurrence of electron injection from the excited state of **Ru** into HCa$_2$Nb$_3$O$_{10}$. Note that these experiments assessed the electron injection process not only from the ^{3}MLCT excited-state but also from ^{1}MLCT, which is known to be an ultrafast process that occurs within a timescale of several hundreds of fs.[2,3]

The single-photon counting method was employed for measuring the decay of emission which was monitored at 630 nm after selective excitation of **Ru** at 444 nm. Fig. 3 shows decay curves of emission from **Ru** adsorbed on layered HCa$_2$Nb$_3$O$_{10}$ and the nanosheets prepared by the PC method. As a reference,
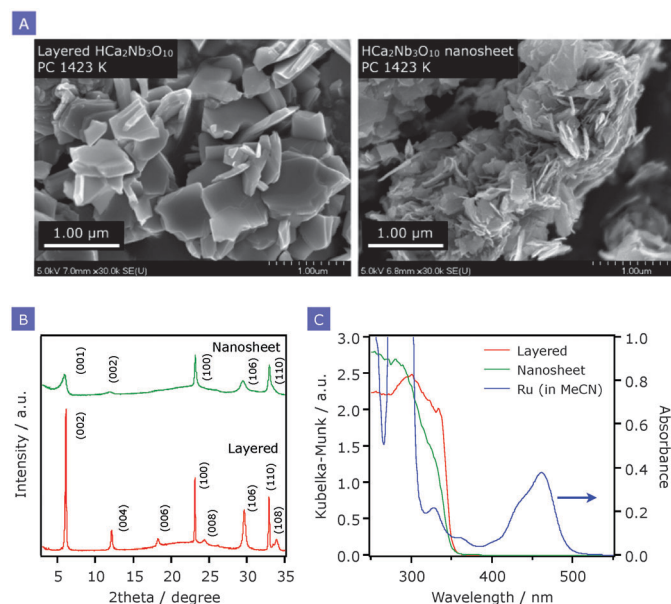

Fig. 1 (A) SEM images, (B) X-ray diffraction patterns, and (C) UV-visible diffuse reflectance spectra of layered HCa$_2$Nb$_3$O$_{10}$ and HCa$_2$Nb$_3$O$_{10}$ nanosheets prepared by the PC method calcined at 1423 K. In panel (C), an absorption spectrum of **Ru** (24 μM) in acetonitrile (MeCN) is shown for comparison.
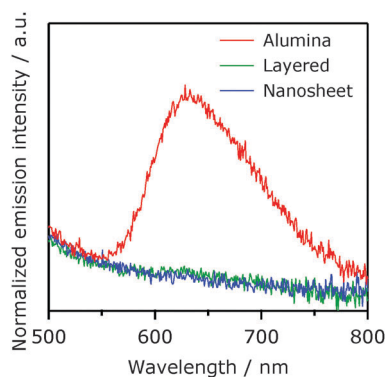

Fig. 2 Steady-state emission spectra of **Ru** on layered HCa$_2$Nb$_3$O$_{10}$ and HCa$_2$Nb$_3$O$_{10}$ nanosheets prepared by the PC method calcined at 1423 K, along with that of **Ru**/Al$_2$O$_3$ for reference. The spectra were obtained by 444 nm photoexcitation. Note that reductive quenching of the ^{3}MLCT excited state of **Ru** by EDTA does not occur.
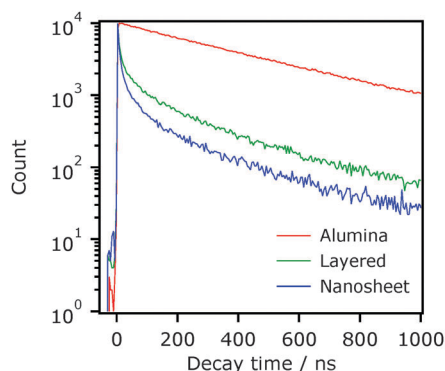
This journal is © the Owner Societies 2015

Phys. Chem. Chem. Phys., 2015, **17**, 17962–17966 | **17963**

Fig. 3 Emission decay curves of **Ru** on layered $HCa_2Nb_3O_{10}$ and $HCa_2Nb_3O_{10}$ nanosheets prepared by the PC method calcined at 1423 K. Excited at 444 nm and monitored at 630 nm, along with that of **Ru**/Al_2O_3 for reference. For each sample, the measurement was repeated until the signal count just after photoexcitation (at $t = 0$) reached 10^4.

data on **Ru**/Al_2O_3 are also shown. Note that due to the time resolution of our apparatus (> 200 ps), the observed emission decay is attributed to emission from the lowest ^{3}MLCT excited state.[20] Electron injection from the excited state of **Ru** into Al_2O_3 does not proceed because of the insulating nature of Al_2O_3. It is clear that the emission decay of **Ru** was more pronounced on the two $HCa_2Nb_3O_{10}$ materials than on Al_2O_3, indicating the occurrence of electron injection from the excited state of **Ru** into the $HCa_2Nb_3O_{10}$ materials, consistent with the result of steady-state emission spectroscopy (Fig. 2). However, the emission decay of the layered material was relatively slow, whereas the nanosheet material showed a faster decay profile. It should be stressed that this tendency was independent of the preparation condition and method of $HCa_2Nb_3O_{10}$; that is, a faster decay profile was observed in the nanosheet system (Fig. S2, ESI†). The faster emission decay of the nanosheet material indicates the occurrence of faster electron injection. The faster electron injection of the nanosheet system compared to the layered one may seem unreasonable because one can expect an lowered driving force for electron injection due to the enlarged difference between the oxidation potential of the excited state (E_{ox}^*) and E_{CB} upon exfoliation-restacking. Therefore, there is another pathway of electron injection from the excited state of **Ru** into $HCa_2Nb_3O_{10}$. One plausible explanation is that part of electrons from the excited-state of **Ru** are injected not only into the conduction band of the aggregated $HCa_2Nb_3O_{10}$ nanosheets but also into mid-gap states in the material.[2,3] It is known that in an n-type semiconductor including the present niobates, there are mid-gap states located below the conduction band.[3] Here the highly disordered morphological feature of the aggregated $HCa_2Nb_3O_{10}$ nanosheets could contain more defects that give localized states working as electron-accepting levels, compared to the ordered lamellar structured one. This situation would contribute to more efficient electron injection from the excited-state of **Ru** into the aggregated $HCa_2Nb_3O_{10}$ nanosheets.

We also tried to resolve the decay profiles of the same samples. However, it was very difficult especially for the nanosheet material even using four exponential functions, suggesting that **Ru** on the

nanosheet material had different adsorption forms such as protonation/deprotonation of the phosphonate groups in the ligand.

If the idea (electron injection into mid-gap states) is correct, $HCa_2Nb_3O_{10}$ having more structural imperfections will accelerate electron injection from the excited state of **Ru** more efficiently, resulting in a more pronounced emission decay profile. In order to investigate this, we prepared lamellar $HCa_2Nb_3O_{10}$ and the aggregated nanosheets at lower calcination temperature (1023 K). By lowering calcination temperature in the final step of the PC method, one can prepare less-crystallized lamellar $HCa_2Nb_3O_{10}$ and the nanosheet with smaller lateral dimensions, as revealed by our previous work.[12] Here XRD patterns and SEM images of the as-prepared lamellar $HCa_2Nb_3O_{10}$ solids are given in the ESI† (Fig. S3 and S4).

Fig. 4 compares the emission decay profiles of **Ru** on two different $HCa_2Nb_3O_{10}$ nanosheets prepared at 1023 and 1423 K. As expected, lowering the calcination temperature of the PC method from 1423 to 1023 K accelerated the emission decay. This result further supports our claim that **Ru** in the excited state injects an electron not only into the conduction band of $HCa_2Nb_3O_{10}$ but also into mid-gap states.

The behaviour of emission decay of **Ru** on the aggregated $HCa_2Nb_3O_{10}$ nanosheets was further investigated with respect to the preparation method of the nanosheet.[21] Fig. 4 also compares emission decays of **Ru** adsorbed on two different $HCa_2Nb_3O_{10}$ nanosheets, which were prepared by SSR and PC methods at the same calcination temperature (1423 K). Interestingly, a faster decay curve was observed in the sample prepared by the SSR method. This strongly suggests that the SSR-derived material contains more mid-gap states than the PC material. However, this may seem to contradict the results of structural characterization; *i.e.*, the intensity of diffraction peaks of the SSR sample is much stronger than that of the PC sample, indicating that more pronounced crystallization occurred in the former (Fig. S3 and S4, ESI†). Nevertheless, it is known that the PC method allows one to obtain metal oxides with lower density of defects and/or vacancies even at lower temperatures, compared to a conventional SSR method.[22,23] Accordingly, we believe that a slower emission decay profile recorded in the PC sample is reasonable.
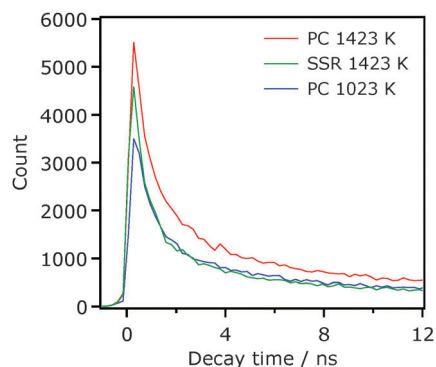

Fig. 4 Emission decay curves of **Ru** on $HCa_2Nb_3O_{10}$ nanosheets prepared by different methods. Excited at 444 nm and monitored at 630 nm, along with that of **Ru**/Al_2O_3 for reference. Each measurement was conducted by irradiating the sample cell with a fixed number of photons.

Conclusions

In summary, even though the conduction band potential of aggregated $HCa_2Nb_3O_{10}$ nanosheets is slightly more negative than that of lamellar $HCa_2Nb_3O_{10}$, electron injection from the excited state of **Ru** is faster in the former than in the latter. Mid-gap states in the $HCa_2Nb_3O_{10}$ nanosheets are suggested to accept electrons from the excited state of **Ru**, thereby facilitating the emission decay of **Ru**. Although it was believed that the E_{CB} of a semiconductor primarily determines the driving force for electron injection from the excited state of a redox photosensitizer, this is the first experimental result that strongly suggests significant contribution of mid-gap states existing in a semiconductor to the charge injection process. Mid-gap states that originate from defects and/or vacancies in a semiconductor solid are known to have a strong impact on photocatalytic activity of the semiconductor.[24,25] Therefore, the present result may be useful as a probe to assess the density of defects and/or vacancies. Our research is now under way along this line.

Experimental section

Preparation of layered $HCa_2Nb_3O_{10}$

First, $KCa_2Nb_3O_{10}$ was synthesized by the polymerized complex method according to our previous papers.[12,13] The final calcination temperature of the PC method varied from 1023 to 1423 K in order to control the size of lateral dimensions of 2D sheets. The detailed characterization data can be found in our previous paper. Then, the as-prepared $KCa_2Nb_3O_{10}$ was subject to proton exchange with 1 M HNO_3 (100 mL) for 6–7 days, followed by centrifugation to separate the resulting solid, which was washed with pure water until the pH of the supernatant became neutral.

$KCa_2Nb_3O_{10}$ was also prepared by a solid-state reaction method according to a previous report.[18] K_2CO_3 ($\geq$99.5%, Kanto Chemical Co.), $CaCO_3$ ($\geq$99.5%, Kanto Chemical Co.), and Nb_2O_5 ($\geq$99.95%, Kanto Chemical Co.) were mixed with an agate mortar and pestle at a molar ratio of K/Ca/Nb = 1.1/2/3, and the mixture was calcined in air at 1123 K for 1 h. An excess of K_2CO_3 (10 mol% excess K) was added to compensate for loss due to volatilization. After cooling to room temperature, the sample was mixed again, and was calcined in air at 1423 K for 10 h. The as-prepared material was subject to proton-exchange in the same manner.

Elemental analysis by means of energy-dispersive X-ray spectroscopy (EDS) showed that approximately 95% of K^+ ions in the interlayer space were exchanged with protons. For simplicity, the obtained products will be referred to as $HCa_2Nb_3O_{10}$.

Preparation of aggregated $HCa_2Nb_3O_{10}$ nanosheets

Layered $HCa_2Nb_3O_{10}$ samples were treated with an aqueous TBAOH solution to exfoliate the layered structure. The molar ratio of TBA^+ cations to exchangeable cations was 1 by mole. After shaking the suspension for 6–7 days, the resulting colloidal solution was allowed to stand for 1 day to precipitate the unreacted portion. After removal of the unreacted solids, the resulting

nanosheet suspension was reassembled by adding HCl, followed by washing with H_2O in a similar manner.

Adsorption of Ru complexes

$Ru\{(4,4'-(CH_3)_2\text{-bpy})_2(4,4'-(CH_2PO_3H_2)_2\text{-bpy})\}(PF_6)_2$ (bpy = 2,2'-bipyridine), abbreviated as **Ru** in this work, was synthesized according to the previous literature with some modifications.[26,27] It was confirmed by ^{1}H-NMR spectroscopy, electrospray ionization-mass spectroscopy (ESI-MS) and elemental analysis that the complexes were successfully synthesized.

The as-prepared $HCa_2Nb_3O_{10}$ lamellar solid or aggregated nanosheet (20 mg) was suspended in acetonitrile containing **Ru** (total volume, 10 mL). After magnetically stirring overnight in the dark, the suspension was filtered, and the resulting pale-orange powder was collected. Finally, the collected powder was dried in an oven at 343 K overnight. The amount of adsorbed **Ru** sensitizers onto a given substrate was estimated by using the following equation:

$$\text{Adsorbed amount } (\mu mol\ g^{-1}) = \frac{A_{before} - A_{after}}{A_{before}}$$
$$\cdot \frac{C\ (\mu mol\ L^{-1}) \times 10 \times 10^{-3}\ (L)}{20 \times 10^{-3}\ (g)}$$

where A_{before} and A_{after} indicate the absorbance of **Ru** in a test solution at the ^{3}MLCT maximum wavelength before and after the adsorption procedure, and C is the concentration of the complex in the solution before adsorption, respectively.

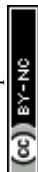### Steady-state emission spectroscopy

Steady-state emission spectra were acquired using a multichannel spectrometer attached to a calibrated integrating sphere (C9920-02G, Hamamatsu Photonics) under 444 nm excitation at room temperature. The measurements were conducted by dispersing a 5.0 mg of the powdered sample adsorbed with **Ru** (2.0 μmol g^{-1}) in 3.0 mL of 10 mM EDTA aqueous solution under an Ar atmosphere.

Time-resolved emission spectroscopy

Emission decay monitored at 630 nm, corresponding to the emission from **Ru**, was measured by the time-dependent single photon counting method using a FluoroCube 1000U-S spectrofluorometer under 444 nm photoexcitation (NanoLED-440L, HORIBA) with a TBX-04 detector at room temperature. A 5.0 mg of **Ru**/$HCa_2Nb_3O_{10}$ powder was dispersed in 3.0 mL of 10 mM EDTA aqueous solution with continuous magnetic stirring under an Ar atmosphere.

This journal is © the Owner Societies 2015

Phys. Chem. Chem. Phys., 2015, **17**, 17962–17966 | **17965**

Notes and references

1 A. Hagfeldt, G. Boschloo, L. Sun, L. Kloo and H. Pettersson, *Chem. Rev.*, 2010, **110**, 6595, and references therein.

2 R. Huber, S. Sebastian Spörlein, J. E. Moser, M. Grätzel and J. Wachtveitl, *J. Phys. Chem. B*, 2000, **104**, 8995.

3 A. Furube, R. Katoh, K. Hara, S. Murata, H. Arakawa and M. Tachiya, *J. Phys. Chem. B*, 2003, **107**, 4162.

4 R. Katoh, A. Furube, T. Yoshihara, K. Hara, G. Fujihashi, S. Takano, S. Murata, H. Arakawa and M. Tachiya, *J. Phys. Chem. B*, 2004, **108**, 4818.

5 V. H. Houlding and M. Grätzel, *J. Am. Chem. Soc.*, 1983, **105**, 5695.

6 Y.-I. Kim, S. Salim, M. J. Huq and T. E. Mallouk, *J. Am. Chem. Soc.*, 1991, **113**, 9561.

7 E. Bae, W. Choi, J. Park, H. S. Shin, S. B. Kim and J. S. Lee, *J. Phys. Chem. B*, 2004, **108**, 14093.

8 Q. Li, Z. Jin, Z. Peng, Y. Li, S. Li and G. Lu, *J. Phys. Chem. C*, 2007, **111**, 8237.

9 R. Abe, K. Shinmei, K. Hara and B. Ohtani, *Chem. Commun.*, 2009, 3577.

10 K. Maeda, M. Eguchi, W. J. Youngblood and T. E. Mallouk, *Chem. Mater.*, 2008, **20**, 6770.

11 K. Maeda, M. Eguchi, S.-H. A. Lee, W. J. Youngblood, H. Hata and T. E. Mallouk, *J. Phys. Chem. C*, 2009, **113**, 7962.

12 K. Maeda, M. Eguchi, W. J. Youngblood and T. E. Mallouk, *Chem. Mater.*, 2009, **21**, 3611.

13 K. Maeda, G. Sahara, M. Eguchi and O. Ishitani, *ACS Catal.*, 2015, **5**, 1700.

14 M. M. Maitani, K. Tanaka, D. Mochizuki and Y. Wada, *J. Phys. Chem. Lett.*, 2011, **2**, 2655.

15 K. Hashimoto, M. Hiramoto, T. Sakata, H. Muraki, H. Takemura and M. Fujihira, *J. Phys. Chem.*, 1987, **91**, 6198.

16 W. E. Ford, J. M. Wessels and M. A. J. Rodgers, *Langmuir*, 1996, **12**, 3449.

17 C.-W. Chang, C. K. Chou, I. Chang, Y.-P. Lee and E. W. Diau, *J. Phys. Chem. C*, 2007, **111**, 13288.

18 T. Oshima, O. Ishitani and K. Maeda, *Adv. Mater. Interfaces*, 2014, **1**, 1400131.

19 F. E. Osterloh, *Chem. Soc. Rev.*, 2013, **42**, 2294.

20 T. Yui, H. Takeda, Y. Ueda, K. Sekizawa, K. Koike, S. Inagaki and O. Ishitani, *ACS Appl. Mater. Interfaces*, 2014, **6**, 1992.

21 Here, the integration of the signal count profile from $t = 0$ (just after photoexcitation) to $t = \infty$ corresponds, in principle, to the emission quantum yield. Therefore, time-resolved emission measurement should be done in this way. Due to different morphological characteristics of different materials, however, the y-axis count depends on the material employed. To avoid this complication, we normalized data obtained using different materials by repeating the measurement until the signal count reached 10 000 (Fig. 3). Nevertheless, we should be able to apply this way (irradiation with a fixed number of photons) when we compare materials with similar structural features. That is why we used different representations in the y axis shown in Fig. 4. Actually, the nanosheet materials shown in Fig. 4 have rough surface structures with almost the same surface area (approximately 50 m^2 g^{-1}). We wish to point out that the direct measurement of emission strength cannot be employed for determining the emission quantum yield because light scattering by the nanosheet should cause disunity of the number of photons absorbed by the **Ru** complex.

22 M. Kakihana, *J. Sol-Gel Sci. Technol.*, 1996, **5**, 7.

23 S. Ikeda, M. Hara, J. N. Kondo and K. Domen, *Chem. Mater.*, 1998, **10**, 72.

24 S. Ikeda, N. Sugiyama, S.-y. Murakami, H. Kominami, Y. Kera, H. Noguchi, K. Uosaki, T. Torimoto and B. Ohtani, *Phys. Chem. Chem. Phys.*, 2003, **5**, 778.

25 K. Maeda, N. Murakami and T. Ohno, *J. Phys. Chem. C*, 2014, **118**, 9093.

26 B. Gholamkhass, H. Mametsuka, K. Koike, M. Furue and O. Ishitani, *Inorg. Chem.*, 2005, **44**, 2326.

27 M. R. Norris, J. J. Concepcion, C. R. K. Glasson, Z. Fang, A. M. Lapides, D. L. Ashford, J. L. Templeton and T. J. Meyer, *Inorg. Chem.*, 2013, **52**, 12492.

17966 | *Phys. Chem. Chem. Phys.*, 2015, **17**, 17962–17966

This journal is © the Owner Societies 2015